Geophysical Research Letters

RESEARCH LETTER
10.1029/2018GL079259

Atomic Oxygen Abundance Retrieved From SCIAMACHY Hydroxyl Nightglow Measurements

Yajun Zhu[1] and Martin Kaufmann[1,2]

[1]Institute of Energy and Climate Research, Forschungszentrum Jülich, Jülich, Germany, [2]Institute for Atmospheric and Environmental Research, University of Wuppertal, Wuppertal, Germany

Key Points:
- A new atomic oxygen data set based on SCIAMACHY OH nightglow measurements at the mesopause is presented
- New data build a consistent picture with SCIAMACHY O(^{1}S) green line and latest SABER data
- Reaction between atomic oxygen and ozone is indispensable in the photochemical model

Correspondence to:
M. Kaufmann,
m.kaufmann@fz-juelich.de

Citation:
Zhu, Y., & Kaufmann, M. (2018). Atomic oxygen abundance retrieved from SCIAMACHY hydroxyl nightglow measurements. *Geophysical Research Letters*, *45*, 9314–9322. https://doi.org/10.1029/2018GL079259

Received 18 JUN 2018
Accepted 13 AUG 2018
Accepted article online 23 AUG 2018
Published online 14 SEP 2018

Abstract We present a new atomic oxygen data set based on Scanning Imaging Absorption Spectrometer for Atmospheric CHartographY (SCIAMACHY) hydroxyl short-wave infrared data. The OH spectra stem from the OH(9-6) ro-vibrational transition. These data and atomic oxygen obtained from SCIAMACHY O(^{1}S) green line measurements, which is an independent data set in terms of methodology and radiometry, typically agree within 10–20%. This confirms the corresponding models of OH and O(^{1}S), in particular, the relevance of the reaction between atomic oxygen and ozone in the photochemical model. The agreement between the SCIAMACHY data and the most recent Sounding of the Atmosphere using Broadband Emission Radiometry (SABER) atomic oxygen data set of Mlynczak et al. (2018, https://doi.org/10.1029/2018GL077377) is significantly better than for the previous SABER data set of Mlynczak et al. (2013, https://doi.org/10.1002/jgrd.50401). The agreement decreases if the SCIAMACHY forward model parameters are applied to SABER data. A similar agreement is achieved with the data of Panka et al. (2018, https://doi.org/10.1029/2018GL077677), which was retrieved from SABER data using a principally different retrieval approach.

Plain Language Summary The latest model and laboratory findings on the relaxation of vibrationally excited OH and the wide distribution of recent satellite data have sparked debate on the abundance of atomic oxygen and its impact on the energy balance of the mesopause region. The debate began with the large values originally derived from Sounding of the Atmosphere using Broadband Emission Radiometry (SABER) OH measurements in 2013 and significantly smaller values obtained from Scanning Imaging Absorption Spectrometer for Atmospheric CHartographY (SCIAMACHY) O(^{1}S) observations in 2014. This confused our understanding of the energy balance of the upper atmosphere and affects the retrieval of several other constituents (temperature, CO_2, O_3, etc.), which rely on atomic oxygen a priori data. In this work we present a new atomic oxygen data set based on SCIAMACHY hydroxyl short-wave infrared data. These data and atomic oxygen obtained from SCIAMACHY O(^{1}S) green line measurements, which is an independent data set in terms of methodology and radiometry, typically agree within 10–20%. This confirms the corresponding models of OH and O(^{1}S), in particular, the relevance of the reaction between atomic oxygen and ozone in the photochemical model.The agreement between the SCIAMACHY and the most recent SABER atomic oxygen data sets of Mlynczak et al. (2018, https://doi.org/10.1029/2018GL077377) and Panka et al. (2018, https://doi.org/10.1029/2018GL077677) is significantly better than for the previous SABER data set.

1. Introduction

Atomic oxygen plays a crucial role in the photochemistry and energy balance of the UMLT (upper mesosphere and lower thermosphere) region (Brasseur & Offermann, 1986; Mlynczak & Solomon, 1993; Riese et al., 1994). Atomic oxygen is mainly produced by the photolysis of molecular oxygen in the thermosphere during daytime due to the absorption of solar ultraviolet radiation. The downward transport of this species through advection and diffusion plays an important role in the spatial distribution of atomic oxygen in that region (Smith & Marsh, 2005). Atomic oxygen is the most abundant reactive species in the UMLT, and its exothermic recombination reactions dominate chemical heating. In addition, knowledge of atomic oxygen is indispensable for the derivation of temperature, CO_2, ozone, and other constituents in the UMLT. Therefore, it is essential to know the atomic oxygen abundance with absolute accuracy.

The only direct measurements of atomic oxygen were performed by in situ instrumentation on sounding rockets (Dickinson et al., 1980; Offermann et al., 1981; Trinks et al., 1978). Global measurements of atomic oxygen rely on species involved in the photochemistry of this species, such as ozone or the various excited states of molecular and atomic oxygen, and can be derived from these data by means of photochemical models. A key reaction in this context is the three-body recombination reaction of atomic oxygen ($O + O + M \rightarrow O_2^* + M$) leading to highly excited molecular oxygen. This metastable state is quenched by atomic or molecular oxygen, whose products radiate nightglow and dayglow. The $O(^1S)$ green line and O_2 A-band emissions are frequently used as proxies for the atomic oxygen abundance. The $O(^1S)$ green line nightglow was measured by the WINDII (Wind Imaging Interferometer) instrument on board the Upper Atmosphere Research Satellite from 1991 to 1997 (Russell et al., 2005) and by the SCIAMACHY (Scanning Imaging Absorption Spectrometer for Atmospheric CHartographY) instrument on the Envisat (Environmental Satellite) from 2002 to 2012 (Kaufmann et al., 2014; Zhu et al., 2015), as well as by the Imager of Sprites and Upper Atmospheric Lightning instrument on board the FORMOSAT-2 satellite (Gao et al., 2012). O_2 A-band dayglow and nightglow measurements were performed by the Optical Spectrograph and Infrared Imager System instrument on the Odin satellite (Sheese et al., 2011).

A different method to determine the atomic oxygen abundance is to observe vibrationally excited OH emissions. The hydroxyl radical is produced in the chemical reaction of ozone and atomic hydrogen, which is the major ozone loss reaction at nighttime. Atomic oxygen can be derived from the balance of ozone loss and ozone production via the three-body recombination reaction of atomic oxygen and molecular oxygen ($O + O_2 + M \rightarrow O_3 + M$). This method was applied to the OH measurements of WINDII (Russell & Lowe, 2003; Russell et al., 2005) and SABER (Sounding of the Atmosphere using Broadband Emission Radiometry) (Mlynczak et al., 2013, 2018). References to other satellite and rocket borne data sets are made in the studies mentioned above.

The abundance of atomic oxygen has long been a subject of discussion. Recent satellite data sets have stimulated a resurgence of the discussion and new laboratory findings on the relaxation of vibrationally exited OH can shed a new light on the current discrepancies.

2. SCIAMACHY OH and Auxiliary Data

In this study we present a new atomic oxygen data set based on hydroxyl Meinel band near-infrared emission measurements performed by SCIAMACHY on Envisat from 2002 to 2012. The spectral range of the instrument covers a multitude of OH emission bands (Kaufmann et al., 2008) ranging from the visible to the near infrared region. For the following study, we use data at wavelengths between 1,377 and 1,400 nm (Figure 1) at a spectral resolution of 1.5 nm from SCIAMACHY channel 6. This is the same spectral region used by Kaufmann et al. (2013) for the derivation of atomic hydrogen abundances from SCIAMACHY data. It covers ro-vibrational lines from the OH(9–6) vibrational transition with low rotational quantum numbers N ($N \leq 3$). The advantages are as follows: First, the excitation of the emitting state is independent of the detailed quenching scheme applied in the model, which becomes more relevant for lower vibrational states. Second, the restriction to ro-vibrational states with low N numbers avoids the potential uncertainty caused by overpopulated high-N rotational states, which have recently been observed (Cosby & Slanger, 2007; Noll et al., 2015; Oliva et al., 2015). And third, SCIAMACHY channel 6 is considered to be a well-understood and well-calibrated channel.

Envisat operates in a Sun-synchronous orbit at an equator crossing local solar time of 10 a.m./p.m. In order to enhance the signal-to-noise ratio and to obtain a high number of coincident measurements with the TIMED (Thermosphere Ionosphere Mesosphere Energetics Dynamics) satellite, monthly zonal median data in 5° latitude bins are used in this study. Since the SCIAMACHY instrument cannot measure nighttime ozone, temperature, or total density in the UMLT, colocated SABER measurements (v2.0) are used here. These atmospheric quantities were derived using the atomic oxygen data of Mlynczak et al. (2013) merged with model data above 90 km. The coincidence criteria are ±2.5° in latitude and 1 hr in local time.

3. OH Nightglow Modeling

The basic procedure for deriving atomic oxygen abundance from hydroxyl nightglow emissions is based on the balance of ozone production and loss at nighttime. This yields the following equation to determine the

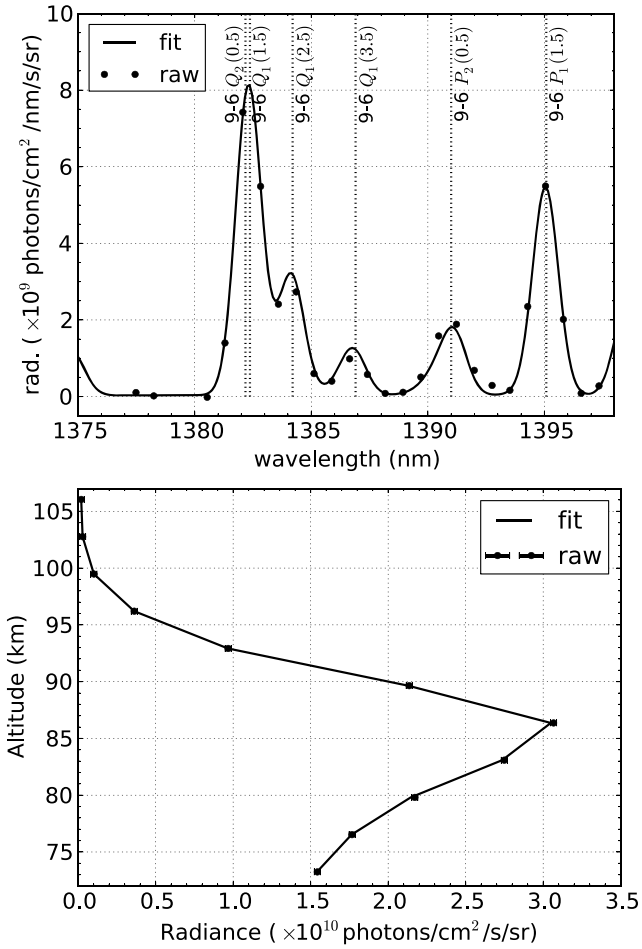

Figure 1. SCIAMACHY monthly zonal mean OH(9-6)-band spectra (top) at a tangent altitude of 86 km for November 2005 at 35–40°N and a local time of 10 p.m. The main OH emission line quantum numbers are given. An altitude profile of spectrally integrated data (1,377–1,400 nm) for the same conditions (bottom). The measurements are plotted as symbols, and the simulation, using retrieved atomic oxygen data, is shown as a solid line. SCIAMACHY = Scanning Imaging Absorption Spectrometer for Atmospheric CHartographY.

atomic oxygen abundance:

$$[O] = \frac{P}{k_1 \cdot [O_2] \cdot [M] - k_3 \cdot [O_3]} \qquad P = k_2 \cdot [H] \cdot [O_3] \tag{1}$$

k_1 is the rate constant for the three-body recombination reaction of O and O_2; k_2 and k_3 are the rate constants for the reactions of H and O with O_3, respectively; [H], [O], [O_2], [O_3], and [M] are the concentrations of atomic hydrogen, atomic oxygen, molecular oxygen, ozone, and the total number density, respectively. k_1, k_2, and k_3 are taken from Sander et al. (2011). P is the total production rate of vibrationally excited OH (OH*). The reaction of atomic oxygen and ozone (second term in the denominator of equation (1), which is a minor ozone loss mechanism, was omitted in the derivation of atomic oxygen from WINDII (Russell & Lowe, 2003) and SABER (Mlynczak et al., 2013, 2018) data. P is derived from the production rate P_9 of OH($v = 9$) considering the fraction f_9 of molecules formed in this vibrational level:

$$P_9 = f_9 \cdot P \tag{2}$$

The production rate P_9 is calculated from the measured emission rates $V(i)$ of a set of ro-vibrational lines within the OH(9-6) vibrational band as follows:

$$P_9 = (A_9 + C_9)\frac{\sum_i V(i)}{\sum_i A_{9-6}(i) \cdot g_9(i) e^{-E(i)/(kT)}/Q_9} \tag{3}$$

Table 1
Quenching Rate Constants of the OH Model*

Process	Rate constant	Factor[a]	Mlynczak et al. (2018)
$OH(9)+N_2$	$(7 \pm 2) \times 10^{-13}$ cm^3/s	1.4	$3.36 \times 10^{-13} e^{220/T}$ cm^3/s
$OH(9)+O_2$	$(2.2 \pm 0.6) \times 10^{-11}$ cm^3/s	1.18	2.5×10^{-11} cm^3/s
OH(9)+O	$(2.3 \pm 1) \times 10^{-10}$ cm^3/s	—	3.0×10^{-10} cm^3/s

[a]A low-temperature-scale factor.

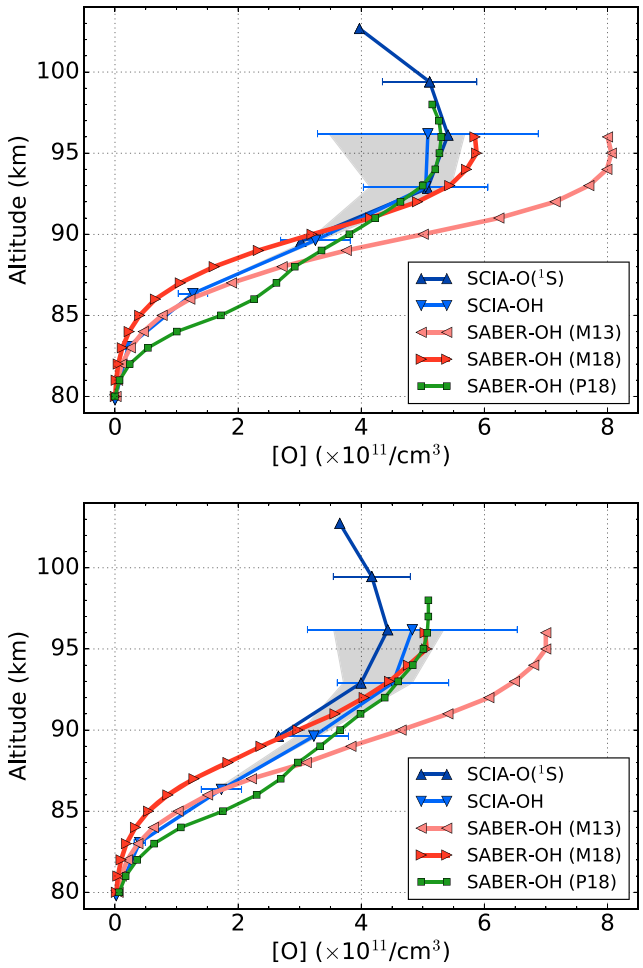

Figure 2. Monthly zonal mean atomic oxygen abundance at 20–50°N for September 2006 (top) and November 2006 (bottom). SCIA-OH = [O] derived from SCIAMACHY OH(9-6)-band emission measurements; SCIA-O(^{1}S) = [O] derived from SCIAMACHY green line measurements. The horizontal lines are error bars considering the uncertainties of rate constants and background atmosphere. The uncertainties of SCIA-O(^{1}S) are similar at lower altitudes. SABER-OH (M13) and SABER-OH (M18) = The SABER atomic oxygen data sets derived by Mlynczak et al. (2013) (M13) and Mlynczak et al. (2018) (M18). The data at the lower bound of the gray area were derived from SCIAMACHY OH(9-6)-band emission measurements using the rate constants of Mlynczak et al. (2018). For the calculation of the data at the upper bound of the gray area, the reaction of O + O_3 was additionally taken into account (which is not considered in the original model of Mlynczak et al. (2018)). SABER-OH (P18) marks the atomic oxygen abundance as retrieved from the two SABER OH channels using the method of Panka et al. (2018). SCIAMACHY = Scanning Imaging Absorption Spectrometer for Atmospheric CHartographY; SABER = Sounding of the Atmosphere using Broadband Emission Radiometry.

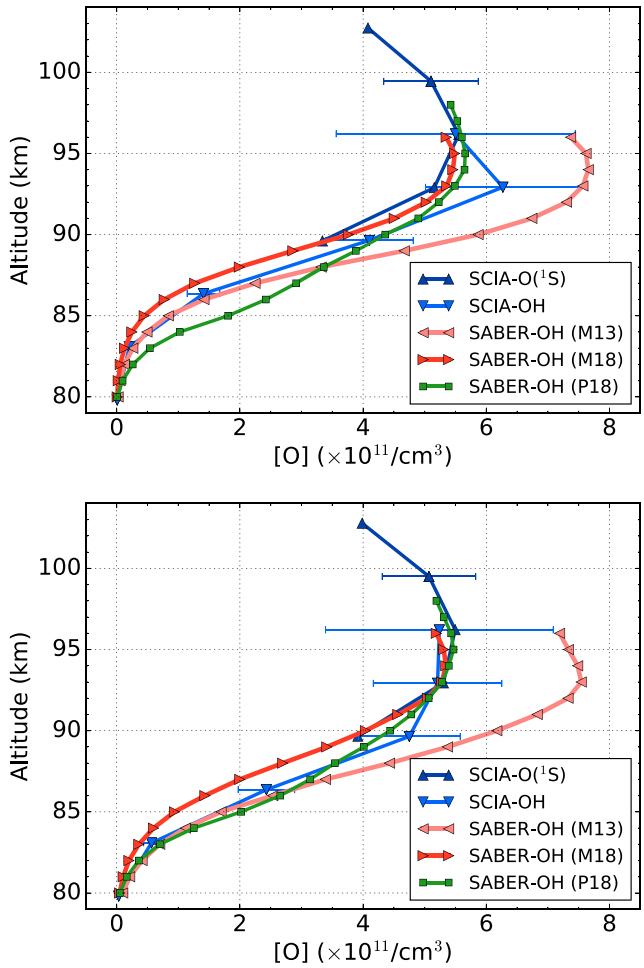

Figure 3. Atomic oxygen profiles for fall 2005 at 20–40°N (top) and 40–60°N (bottom). See Figure 2 for details.

A_9 and C_9 are the sum of all spontaneous emission, quenching, and chemical destruction rates depopulating vibrational level 9, respectively. $V(i)$ and $A_{9-6}(i)$ are the volume emission rate and Einstein coefficient of the ith line within the 9-6 band considered. E and g are the rotational energy and degeneracy of the rotational upper state of the ith line considered. k is Boltzmann factor, and T is temperature. Q_9 is the rotational partition sum of OH($v = 9$).

The model presented in this study uses the quasi-nascent distribution ($f_9 = 0.47$) compiled by Adler-Golden (1997) and the collisional rate constants measured by Kalogerakis et al. (2011). The rate constant of OH($v = 9$) with O_2 is in good agreement with the findings of Xu et al. (2012). In addition, the collisional rate constants of OH($v = 9$) with N_2 and O_2 were scaled by a factor of 1.4 and 1.18, respectively, to account for the low mesopause temperatures, as suggested by Lacoursière et al. (2003) and applied by Panka et al. (2017). The quenching rate constant of OH($v = 9$) with atomic oxygen is taken from recent study of Kalogerakis et al. (2016). The collisional rate constants used in this study are also given in Table 1. The Einstein coefficients used in the model are taken from Rothman et al. (2013). For comparison purposes, we also applied the most recent set of rate constants used by Mlynczak et al. (2018) for the derivation of the latest version of SABER atomic oxygen data.

4. Retrieval Results and Discussion

A constraint global fit retrieval scheme is applied to obtain vertical profiles of atomic oxygen abundance between 80 and 96 km. The regularization was adjusted in such a way that the vertical resolution is similar to the vertical sampling of the measurements, which is about 3 km.

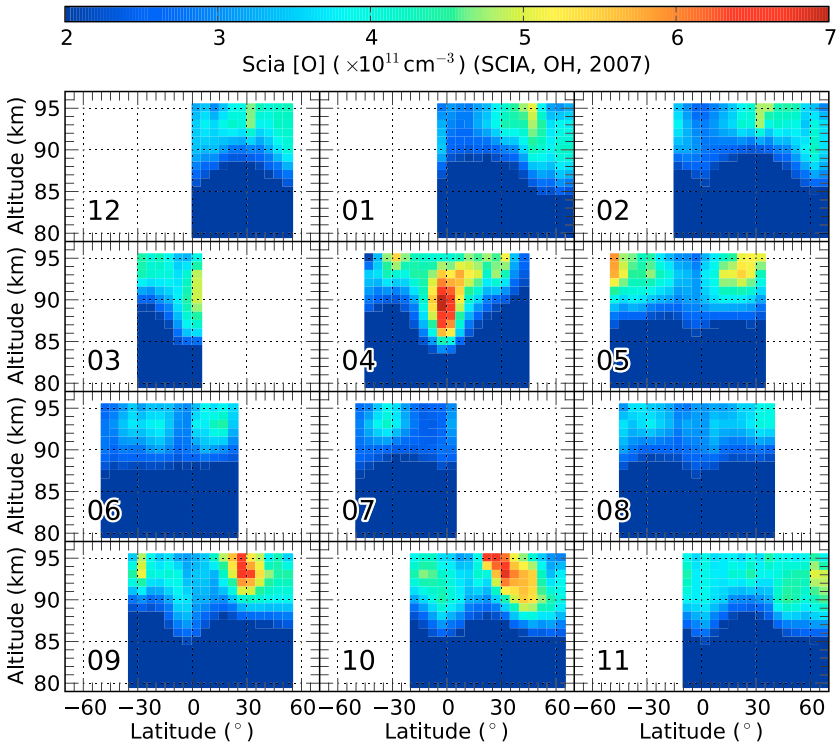

Figure 4. Monthly zonal mean latitude-altitude cross sections of atomic oxygen abundance for 2007, as derived from SCIAMACHY OH(9-6) data. The numbers represent the month of the year.

The confidence level of atomic oxygen was estimated using the uncertainties of the various rate constants and the uncertainties of the auxiliary atmospheric quantities (temperature, ozone, and total density provided by the SABER instrument). Corresponding uncertainties are in the order of 30%, 25%, and 40% for the rate constants describing the quenching by N_2, O_2, and O, respectively. For the atmospheric quantities, a 10% ozone uncertainty is assumed (Smith et al., 2013) and the derived atomic oxygen is most affected at high altitudes (6% at 95 km); SABER temperature uncertainties are about 5 K at 85 km and 9 K at 100 km (García-Comas et al., 2008). This affects total density according to hydrostatic equilibrium and ideal gas law, which counterbalance temperature uncertainties below the mesopause to some extent. Accordingly, atomic oxygen is affected by total density uncertainties by less than 3% below 92 km and 20% at 95 km, only.

Figures 2 and 3 show comparisons between the retrieved atomic oxygen profiles and the atomic oxygen data obtained from SCIAMACHY green line measurements (Kaufmann et al., 2014; Zhu et al., 2015) utilizing the ETON photochemical model (McDade & Llewellyn, 1986). The two data sets overlap in the altitude regime of 90–95 km and agree within 10–20%. The previous and current SABER atomic oxygen data sets (Mlynczak et al., 2013; Mlynczak et al., 2018) are also added for comparison. Since the SABER OH excitation model (reaction rate constants in the photochemical model of ozone and relaxation rate constants in the continuity equation of vibrationally excited OH) differs from the one we used here, the SCIAMACHY data were retrieved using the same model parameters, which is shown in the figure as well.

The spatial distribution of the new atomic oxygen data is illustrated in Figure 4 for the year 2007. The data cover the same period as the atomic oxygen data retrieved from SCIAMACHY O(^{1}S) data shown in Figure 3 of Kaufmann et al. (2014). The comparison of the two data sets from a global perspective (Figure 5) indicates that there is a general negative bias of up to 20% below 93 km for most data points. During the spring and summer seasons, a positive bias of up to 20% in the high altitude for OH-data can be observed in comparison to the O(^{1}S) data. Large deviations of up to 30% are observed in April at midlatitudes in the Southern Hemisphere, but for all other months there are no major systematic differences.

In contrast, the SCIAMACHY data and latest SABER atomic oxygen data set reveal systematic differences at all latitudes and seasons (Figure 5). Below 87 km, the SABER atomic oxygen data set is 40% lower on average than the SCIAMACHY data, which is likely due to the low quenching coefficient of OH(v = 8) with O_2 utilized

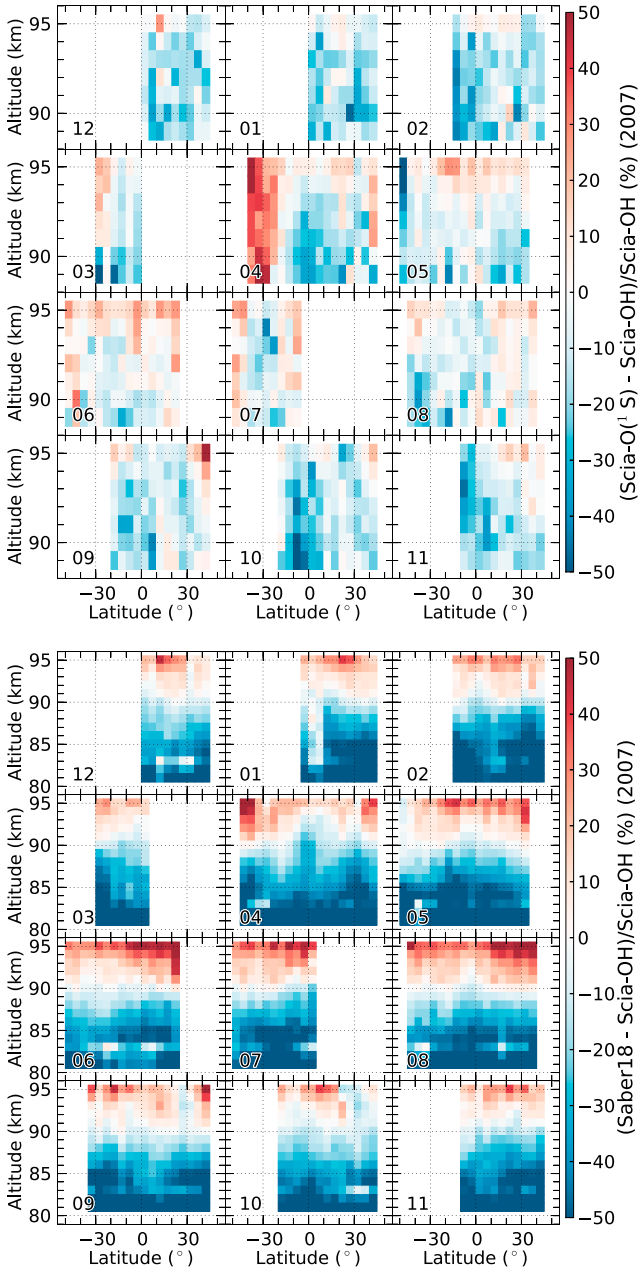

Figure 5. Percentage difference of SCIAMACHY atomic oxygen data for 2007, as derived from O(^{1}S) and OH data (top) and atomic oxygen difference as derived from SCIAMACHY and SABER OH data (bottom). The numbers represent the months of the year. SCIAMACHY = Scanning Imaging Absorption Spectrometer for Atmospheric CHartographY; SABER = Sounding of the Atmosphere using Broadband Emission Radiometry.

in the SABER model (4.8×10^{-13} cm^3/s, Mlynczak et al., 2018). This value is a factor of 50 smaller than the corresponding quenching rate of OH(v = 9). Above 90 km, the difference between the two data sets is reversed, and the SABER atomic oxygen is 10–30% higher. Although the SABER photochemical model of ozone does not take into account the loss of ozone through reaction with atomic oxygen (second term in the denominator of equation (1), which affects retrieved atomic oxygen in the order of 30% at atomic oxygen peak altitudes, the SABER atomic oxygen values are still larger than the SCIAMACHY data. This difference increases further if this process is consistently considered or ignored in both models. We like to point out that we do not observe exceptionally large atomic oxygen abundances in the SCIAMACHY data set if the loss of ozone due to the reaction with atomic oxygen is considered in the model.

Panka et al. (2018) obtained atomic oxygen abundances from SABER OH* observations using a rather different retrieval approach. While the general approach (as used in this study) retrieves most information about atomic oxygen abundance from the absolute radiances of vibrationally excited OH, the method of Panka et al. (2018) relies on the ratio of two radiance channels measuring different vibrationally excited levels of OH. Whereas atomic oxygen affects the radiances in the former case through the chemical equilibrium of ozone at nighttime, it affects the ratio of different OH* channels or the population of different vibrational levels via (multiquantum) quenching. In general, SCIAMACHY data and these data agree as well as the other data sets. At lower altitudes, SCIAMACHY data range between the Mlynczak et al. (2018) and Panka et al. (2018) SABER data sets—at least for the conditions analyzed in this study.

5. Conclusions

Atomic oxygen abundances as derived from SCIAMACHY OH(9-6) ro-vibrational spectra typically agree within 20% of the data obtained from SCIAMACHY green line measurements (Kaufmann et al., 2014). Both data sets combined give a consistent profile of atomic oxygen from 80 to 105 km. The agreement of the data in the overlapping region supports our current understanding of the photochemistry of the corresponding emitting states, namely, the ETON model (McDade & Llewellyn, 1986) for $O(^1S)$ and the OH* rate constants of Kalogerakis et al., (2011, 2016) as well as the relevance of the reaction between atomic oxygen and ozone in the photochemical model of ozone.

The atomic oxygen profiles of the latest SABER atomic oxygen data (Mlynczak et al., 2018; Panka et al., 2018) better fit the SCIAMACHY data than the previous data version, at least at higher altitudes. At lower altitudes, the SABER data of Mlynczak et al. (2018) are up to 50% lower than SCIAMACHY data, which is likely due to the low quenching rates of $OH(v = 8)$ used in the SABER retrieval. The difference at higher altitudes is not understood yet. Atomic oxygen data obtained using the novel retrieval approach of Panka et al. (2018) agree well with the SCIAMACHY data, but further comparisons are needed to make a conclusive statement.

Acknowledgments
The work of Y. Zhu was supported by the 2017 Helmholtz-OCPC-Programme and the International Postdoctoral Exchange Fellowship Program 2017. M. Kaufmann was supported by Forschungszentrum Jülich. We would like to thank Martin Mlynczak, Alexander Kutepov, and Peter A. Panka for providing atomic oxygen abundances retrieved from SABER measurements and helpful discussions. SCIAMACHY data were provided within the Cat-1 project 2515, available at ftp://eoa-dp.eo.esa.int. SABER Version 2.0 data are available at http://saber.gats-inc.com.

References

Adler-Golden, S. (1997). Kinetic parameters for OH nightglow modeling consistent with recent laboratory measurements. *Journal of Geophysical Research*, *102*(A9), 19,969–19,976. https://doi.org/10.1029/97JA01622

Brasseur, G., & Offermann, D. (1986). Recombination of atomic oxygen near the mesopause: Interpretation of rocket data. *Journal of Geophysical Research*, *91*(D10), 10,818–10,824. https://doi.org/10.1029/JD091iD10p10818

Cosby, P. C., & Slanger, T. G. (2007). OH spectroscopy and chemistry investigated with astronomical sky spectra. *Canadian Journal of Physics*, *85*(2), 77–99. https://doi.org/10.1139/p06-088

Dickinson, P. H. G., Bain, W. C., Thomas, L., Williams, E. R., Jenkins, D. B., & Twiddy, N. D. (1980). The determination of the atomic oxygen concentration and associated parameters in the lower ionosphere. *Proceedings of the Royal Society of London A: Mathematical, Physical and Engineering Sciences*, *369*(1738), 379–408. https://doi.org/10.1098/rspa.1980.0006

Gao, H., Nee, J.-B., & Xu, J. (2012). The emission of oxygen green line and density of O atom determined by using ISUAL and SABER measurements. *Annales Geophysicae*, *30*(4), 695–701. https://doi.org/10.5194/angeo-30-695-2012

García-Comas, M., López-Puertas, M., Marshall, B. T., Wintersteiner, P. P., Funke, B., Bermejo-Pantaleón, D., et al. (2008). Errors in Sounding of the Atmosphere using Broadband Emission Radiometry (SABER) kinetic temperature caused by non-local-thermodynamic-equilibrium model parameters. *Journal of Geophysical Research*, *113*, D24106. https://doi.org/10.1029/2008JD010105

Kalogerakis, K. S., Matsiev, D., Sharma, R. D., & Wintersteiner, P. P. (2016). Resolving the mesospheric nighttime 4.3 μm emission puzzle: Laboratory demonstration of new mechanism for OH(v) relaxation. *Geophysical Research Letters*, *43*, 8835–8843. https://doi.org/10.1002/2016GL069645

Kalogerakis, K. S., Smith, G. P., & Copeland, R. A. (2011). Collisional removal of $OH(X^2\Pi, v)$ by O, O_2, O_3, N_2, and CO_2. *Journal of Geophysical Research*, *116*, D20307. https://doi.org/10.1029/2011JD015734

Kaufmann, M., Ern, M., Lehmann, C., & Riese, M. (2013). The response of atomic hydrogen to solar radiation changes. In F. -J. Luebken (Ed.), *Climate and Weather of the Sun-Earth System (CAWSES)* (pp. 171–188). Netherlands: Springer.

Kaufmann, M., Lehmann, C., Hoffmann, L., Funke, B., López-Puertas, M., Savigny, C., & Riese, M. (2008). Chemical heating rates derived from SCIAMACHY vibrationally excited OH limb emission spectra. *Advances in Space Research*, *41*(11), 1914–1920. https://doi.org/10.1016/j.asr.2007.07.045

Kaufmann, M., Zhu, Y., Ern, M., & Riese, M. (2014). Global distribution of atomic oxygen in the mesopause region as derived from SCIAMACHY $O(^1S)$ green line measurements. *Geophysical Research Letters*, *41*, 6274–6280. https://doi.org/10.1002/2014GL060574

Lacoursière, J., Dyer, M. J., & Copeland, R. A. (2003). Temperature dependence of the collisional energy transfer of OH($v = 10$) between 220 and 310 K. *The Journal of Chemical Physics*, *118*(4), 1661–1666. https://doi.org/10.1063/1.1530581

McDade, I. C., & Llewellyn, E. J. (1986). The excitation of $O(^1S)$ and O_2 bands in the nightglow: A brief review and preview. *Canadian Journal of Physics*, *64*(12), 1626–1630. https://doi.org/10.1139/p86-287

Mlynczak, M. G., Hunt, L. A., Mast, J. C., Thomas Marshall, B., Russell, J. M., Smith, A. K., et al. (2013). Atomic oxygen in the mesosphere and lower thermosphere derived from SABER: Algorithm theoretical basis and measurement uncertainty. *Journal of Geophysical Research: Atmospheres*, *118*, 5724–5735. https://doi.org/10.1002/jgrd.50401

Mlynczak, M. G., Hunt, L. A., Russell, J. M., & Thomas, M. B. (2018). Updated SABER night atomic oxygen and implications for SABER ozone and atomic hydrogen. *Geophysical Research Letters*, *45*, 5735–5741. https://doi.org/10.1029/2018GL077377

Mlynczak, M. G., & Solomon, S. (1993). A detailed evaluation of the heating efficiency in the middle atmosphere. *Journal of Geophysical Research*, *98*(D6), 10,517–10,541. https://doi.org/10.1029/93JD00315

Noll, S., Kausch, W., Kimeswenger, S., Unterguggenberger, S., & Jones, A. M. (2015). OH populations and temperatures from simultaneous spectroscopic observations of 25 bands. *Atmospheric Chemistry and Physics*, *15*(7), 3647–3669. https://doi.org/10.5194/acp-15-3647-2015

Offermann, D., Friedrich, V., Ross, P., & Zahn, U. V. (1981). Neutral gas composition measurements between 80 and 120 km. *Planetary and Space Science*, *29*(7), 747–764. https://doi.org/10.1016/0032-0633(81)90046-5

Oliva, E., Origlia, L., Scuderi, S., Benatti, S., Carleo, I., Lapenna, E., et al. (2015). Lines and continuum sky emission in the near infrared: Observational constraints from deep high spectral resolution spectra with GIANO-TNG. *Astronomy & Astrophysics*, *581*, A47. https://doi.org/10.1051/0004-6361/201526291

Panka, P. A., Kutepov, A. A., Kalogerakis, K. S., Janches, D., Russell, J. M., Rezac, L., et al. (2017). Resolving the mesospheric nighttime 4.3 μm emission puzzle: Comparison of the $CO_2(\nu_3)$ and OH(ν) emission models. *Atmospheric Chemistry and Physics*, *17*(16), 9751–9760. https://doi.org/10.5194/acp-17-9751-2017

Panka, P. A., Kutepov, A. A., Rezac, L., Kalogerakis, K. S., Feofilov, A. G., Marsh, D., et al. (2018). Atomic oxygen retrieved from the SABER 2.0 and 1.6 μm radiances using new first-principles nighttime OH(v) model. *Geophysical Research Letters*, *45*, 5798–5803. https://doi.org/10.1029/2018GL077677

Riese, M., Offermann, D., & Brasseur, G. (1994). Energy released by recombination of atomic oxygen and related species at mesopause heights. *Journal of Geophysical Research*, *99*(D7), 14,585–14,593. https://doi.org/10.1029/94JD00356

Rothman, L., Gordon, I., Babikov, Y., Barbe, A., Benner, D. C., Bernath, P., et al. (2013). The HITRAN2012 molecular spectroscopic database. *Journal of Quantitative Spectroscopy and Radiative Transfer*, *130*(0), 4–50. https://doi.org/10.1016/j.jqsrt.2013.07.002 HITRAN2012 special issue.

Russell, J. P., & Lowe, R. P. (2003). Atomic oxygen profiles (80–94 km) derived from Wind Imaging Interferometer/Upper Atmospheric Research Satellite measurements of the hydroxyl airglow: 1. Validation of technique. *Journal of Geophysical Research*, *108*(D21), 4662. https://doi.org/10.1029/2003JD003454

Russell, J. P., Ward, W. E., Lowe, R. P., Roble, R. G., Shepherd, G. G., & Solheim, B. (2005). Atomic oxygen profiles (80 to 115 km) derived from Wind Imaging Interferometer/Upper Atmospheric Research Satellite measurements of the hydroxyl and greenline airglow: Local time-latitude dependence. *Journal of Geophysical Research*, *110*, D15305. https://doi.org/10.1029/2004JD005570

Sander, S. P., Abbatt, J., Barker, J. R., Burkholder, J. B., Friedl, R. R., Golden, D. M., et al. (2011). *Chemical Kinetics and Photochemical Data for Use in Atmospheric Studies: Evaluation Number 17*. Pasadena, CA: Jet Propulsion Laboratory.

Sheese, P. E., McDade, I. C., Gattinger, R. L., & Llewellyn, E. J. (2011). Atomic oxygen densities retrieved from Optical Spectrograph and Infrared Imaging System observations of O_2 A-band airglow emission in the mesosphere and lower thermosphere. *Journal of Geophysical Research*, *116*, D01303. https://doi.org/10.1029/2010JD014640

Smith, A. K., Harvey, V. L., Mlynczak, M. G., Funke, B., García-Comas, M., Hervig, M., et al. (2013). Satellite observations of ozone in the upper mesosphere. *Journal of Geophysical Research: Atmospheres*, *118*, 5803–5821. https://doi.org/10.1002/jgrd.50445

Smith, A. K., & Marsh, D. R. (2005). Processes that account for the ozone maximum at the mesopause. *Journal of Geophysical Research*, *110*, D23305. https://doi.org/10.1029/2005JD006298

Smith, A. K., Marsh, D. R., Mlynczak, M. G., & Mast, J. C. (2010). Temporal variations of atomic oxygen in the upper mesosphere from SABER. *Journal of Geophysical Research*, *115*, D18309. https://doi.org/10.1029/2009JD013434

Trinks, H., Offermann, D., von Zahn, U., & Steinhauer, C. (1978). Neutral composition measurements between 90- and 220-km altitude by rocket-borne mass spectrometer. *Journal of Geophysical Research*, *83*(A5), 2169–2176. https://doi.org/10.1029/JA083iA05p02169

Xu, J., Gao, H., Smith, A. K., & Zhu, Y. (2012). Using TIMED/SABER nightglow observations to investigate hydroxyl emission mechanisms in the mesopause region. *Journal of Geophysical Research*, *117*, D02301. https://doi.org/10.1029/2011JD016342

Zhu, Y., Kaufmann, M., Ern, M., & Riese, M. (2015). Nighttime atomic oxygen in the mesopause region retrieved from SCIAMACHY $O(^1S)$ green line measurements and its response to solar cycle variation. *Journal of Geophysical Research: Space Physics*, *120*, 9057–9073. https://doi.org/10.1002/2015JA021405